Herschel: the first science highlights

LETTER TO THE EDITOR

The *Herschel* Virgo Cluster Survey

IV. Resolved dust analysis of spiral galaxies[*]

M. W. L. Smith[1], C. Vlahakis[2], M. Baes[3], G. J. Bendo[4], S. Bianchi[5], D. J. Bomans[6], A. Boselli[7], M. Clemens[8], E. Corbelli[5], L. Cortese[1], A. Dariush[1], J. I. Davies[1], I. De Looze[3], S. di Serego Alighieri[5], D. Fadda[9], J. Fritz[3], D. A. Garcia-Appadoo[10], G. Gavazzi[11], C. Giovanardi[5], M. Grossi[12], T. M. Hughes[1], L. K. Hunt[5], A. P. Jones[13], S. Madden[14], D. Pierini[15], M. Pohlen[1], S. Sabatini[16], J. Verstappen[3], E. M. Xilouris[17], and S. Zibetti[18]

(Affiliations are available in the online edition)

ABSTRACT

We present a resolved dust analysis of three of the largest angular size spiral galaxies, NGC 4501 and NGC 4567/8, in the *Herschel* Virgo Cluster Survey (HeViCS) science demonstration field. *Herschel* has unprecedented spatial resolution at far-infrared wavelengths and with the PACS and SPIRE instruments samples both sides of the peak in the far infrared spectral energy distribution (SED). We present maps of dust temperature, dust mass, and gas-to-dust ratio, produced by fitting modified black bodies to the SED for each pixel. We find that the distribution of dust temperature in both systems is in the range ~19–22 K and peaks away from the centres of the galaxies. The distribution of dust mass in both systems is symmetrical and exhibits a single peak coincident with the galaxy centres. This Letter provides a first insight into the future analysis possible with a large sample of resolved galaxies to be observed by *Herschel*.

Key words. galaxies: evolution – galaxies: spiral – galaxies: ISM

1. Introduction

Infrared data have been widely used to determine the composition and distribution of dust in galaxies since the launch of IRAS in the 1980s. However, dust masses for nearby galaxies calculated from IRAS 60 and 100 μm measurements were found to be a factor of ten lower than expected when compared to the Milky Way gas-to-dust ratio of 100–200 (Devereux & Young 1990). The Milky Way dust mass was calculated by measuring the depletion of metals from the gaseous phase of the interstellar medium (ISM) and by comparing gas column densities to dust extinction (Whittet 2003), its value implying that most of the dust-mass emits radiation at wavelengths longer than 100 μm (e.g., Devereux & Young 1990). Analyses of data from the *Spitzer* Space Telescope have determined gas-to-dust ratios of ~150 (e.g., Draine et al. 2007). However, these analyses were generally limited by the number, and low signal-to-noise ratio of data at wavelengths greater than 160 μm. These studies therefore had difficulty detecting emission from dust with temperatures lower than 15 K, and their results were biased towards warmer dust temperatures and lower masses. Owing to the difficulties at these wavelengths, high resolution studies of galaxies have been previously limited. These studies are important for understanding how dust interacts with the other phases of the ISM, the sources of dust heating and how the distribution and temperature of dust varies with morphology.

The *Herschel* Space Telescope (Pilbratt et al. 2010), with its two photometric instruments, constrains both sides of the peak in the far infrared spectral energy distribution (SED, see Fig. 1). The Photodetector Array Camera and Spectrometer (PACS, Poglitsch et al. 2010) has three photometric bands at 70, 100, and 160 μm at superior angular resolutions to those provided by *Spitzer*. The Spectral and Photometric Imaging REceiver (SPIRE, Griffin et al. 2010) also has three photometric bands observing simultaneously at 250, 350, and 500 μm with high sensitivity and angular resolution.

The *Herschel* Virgo Cluster Survey (HeViCS[1]) is a *Herschel* open time key program that will observe ~64 deg² of the Virgo cluster. This will provide a large sample of resolved galaxies because about 48 late-type galaxies will be observed by HeViCS with optical diameters larger than 3′. In this Letter, we present an insight into what will be possible with the full HeViCS survey by applying a resolved dust analysis to infer dust temperatures, surface densities, and gas-to-dust ratios for NGC 4501 and NGC 4567/8. These galaxies were chosen because they are among the largest angular size systems in the HeViCS science demonstration phase (SDP) field. In Sect. 2, we present the observations and data reduction, and in Sects. 3 and 4, we present our analysis and results, respectively.

2. Observations and data reduction

As part of the *Herschel* SDP, a 4 × 4 sq deg field of the Virgo cluster centred approximately on M 87 has been observed in

---

[*] *Herschel* is an ESA space observatory with science instruments provided by European-led Principal Investigator consortia and with important participation from NASA.

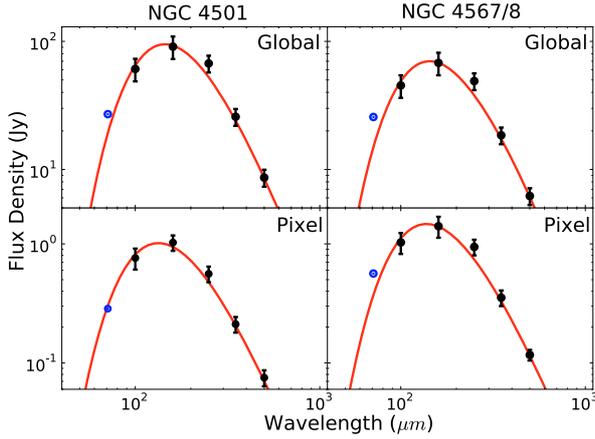[1] More details on HeViCS can be found at http://www.hevics.org

Fig. 1. Global and example single pixel one component SED fits. If not shown, uncertainties are smaller than the symbol size. The 70 μm point (blue) is used as an upper limit (see Sect. 3).

parallel mode, simultaneously at 100 and 160 μm with PACS and at 250, 350, and 500 μm with SPIRE. For details of the observing strategy and data reduction, we refer to Davies et al. (2010). Following the recommendations given by the PACS and SPIRE instrument control centres (ICCs), the 100 and 160 μm PACS flux densities were scaled by dividing by 1.06 and 1.29, respectively, and SPIRE flux densities by multiplying by 1.02, 1.05, and 0.94 for the 250, 350, and 500 μm bands, respectively. The point spread function (PSF) of the PACS images has a *FWHM* of 12.70″ × 6.98″ and 15.65″ × 11.64″ in the 100 μm and 160 μm band, respectively (where the orientation depends on scan direction). The SPIRE PSF has a *FWHM* of 18.1″, 25.2″, and 36.9″ at 250 μm, 350 μm, and 500 μm, respectively. The calibration error is assumed to be 20% for the PACS band and 15% for the SPIRE bands. The PACS and SPIRE images are shown in Figs. 2 and 3.

This Letter focuses on NGC 4501, which is an Sbc galaxy and has an optical diameter (major axis) of 7.23′, and the galaxy pair NGC 4567/8, which are both of Sc type with optical diameters of 2.92′ and 5.1′, respectively (values taken from GOLD Mine; Gavazzi et al. 2003). As NGC 4501 is on the edge of the SDP field, observations were only obtained in one scan direction.

In addition to the *Herschel* data, we used *Spitzer* 70 μm data from Kennicutt et al. (2003), Kenney et al. (2006), and Struck et al. (2004), which were reprocessed using the techniques described in Bendo et al. (2010b). The calibration uncertainty were assumed to be 5% at 70 μm (Gordon et al. 2007). We also use GALEX FUV ($\lambda = 1539$Å, $\Delta\lambda = 442$ Å) data downloaded from the MAST (G4/5) archive. For both NGC 4501 and NGC 4567/8, we used H I maps from the VIVA H I survey (Chung et al. 2009), and for NGC 4501 we also used CO($J = 1$–0) maps from the Nobeyama CO ATLAS survey (Kuno et al. 2007). The H I and CO images are shown in Figs. 2 and 3. For NGC 4567/8, we used global CO($J = 1$–0) measurements from Iono et al. (2005). In the following analysis, neutral atomic hydrogen masses were calculated using $M_{HI} = 2.36 \times 10^5 \, D^2_{Mpc} \mathrm{FI}(M_\odot)$, where FI is the integrated HI line flux in units of Jy km s^{-1} (Roberts 1962) and D_{Mpc} is the distance in Mpc. We assumed the distance to the centre of the M 87 cloud in the Virgo cluster given by Mei et al. (2007) of 16.7 Mpc. To convert a CO integrated line intensity to a value of molecular hydrogen column density, we assume an X factor of 1.9×10^{20} cm^{-2}[K km s^{-1}]$^{-1}$ derived from

Strong & Mattox (1996) using models of gamma ray scattering. However, we note that the value of the X factor is notoriously uncertain and may also vary, for example with metallicity (e.g., Israel 2000).

3. Analysis

We fit simple models to the SEDs of each pixel in our galaxies to produce maps of estimated dust temperature and dust mass. All images were first convolved to the resolution of the 500 μm image (which has a PSF of the largest *FWHM*), using a customised kernel created using the procedure outlined in Bendo et al. (2010b). The images were then regridded to the 14″ pixel size of the 500 μm map. We note that since the pixel size is smaller than the 500 μm beam size, neighbouring pixels are not independent. Owing to lower sensitivities in the PACS 100 μm band and negative artifacts created around the galaxy during the current PACS data reduction process, we only consider pixels with a flux density >10σ in the convolved and regridded 100 μm image; the estimated sensitivities are 7.3 mJy pix^{-1} for the cross-scan region and 10.4 mJy pix^{-1} for the single scan (see Davies et al. 2010 for optimal resolution sensitivities). Thus, in the present work we do not study the outermost regions of the galaxies; the full galaxy extent will be considered in future works.

We fit the SEDs in the 70–500 μm range with one and two component modified black-body models. The equation for a one component black body is given by

$$F_\nu = \frac{\kappa_\nu}{D^2} M B_\nu(T) \cdot \qquad (1)$$

Here M is the dust mass, T is the dust temperature, $B_\nu(T)$ is the Plank function, D is the distance to the galaxy (see Sect. 2), and κ_ν is the dust emissivity. The dust emissivity is assumed to be a power law in this spectral range, where $\kappa_\nu \propto \nu^\beta$. We assume a value of $\kappa_0 = 0.192$ m^2 kg^{-1} at 350 μm (Draine 2003) and $\beta = 2$, though we note that the values of κ and β are notoriously uncertain. The best-fit solution is found by minimising the chi-squared (χ^2) function. To adjust for the filter-band passes, the SED is convolved with the filter transmission in the fitting process.

We find that the data in the 100-500 μm range is accurately fitted by a single black-body component. However, for the majority of pixels a significant flux excess is measured at 70 μm relative to this fit. This indicates that a warmer dust component is present, which is consistent with the results found by Bendo et al. (2010a). A two-component model provides a good fit by using the same component through the 100–500 μm data as the one-component model and adding a warm component that fits the 70 μm emission. The warm component, however, is not tightly constrained since a wide range of warm temperatures statistically provide equally good fits, due mainly to the small number of data points on the Wien side of the SED. Therefore, in this work we choose to use a one-component model with the 70 μm data point as an upper limit. This choice has little effect on the total dust mass since the cold component dominates the dust mass. Example global and single-pixel SEDs are shown in Fig. 1. We note that for most of the SED fits a ~1σ excess is found for the 250 μm band, for which we do not find any immediate explanation and we plan future investigations.

In addition to maps of dust temperature, we also produced maps of dust mass surface density and the gas-to-dust ratio. For NGC 4501, we calculated $M_{gas} = M_{HI} + M_{H_2}$; for NGC 4567/8, we do not have a CO($J = 1$–0) map, so we only consider the H I component of the gas mass.
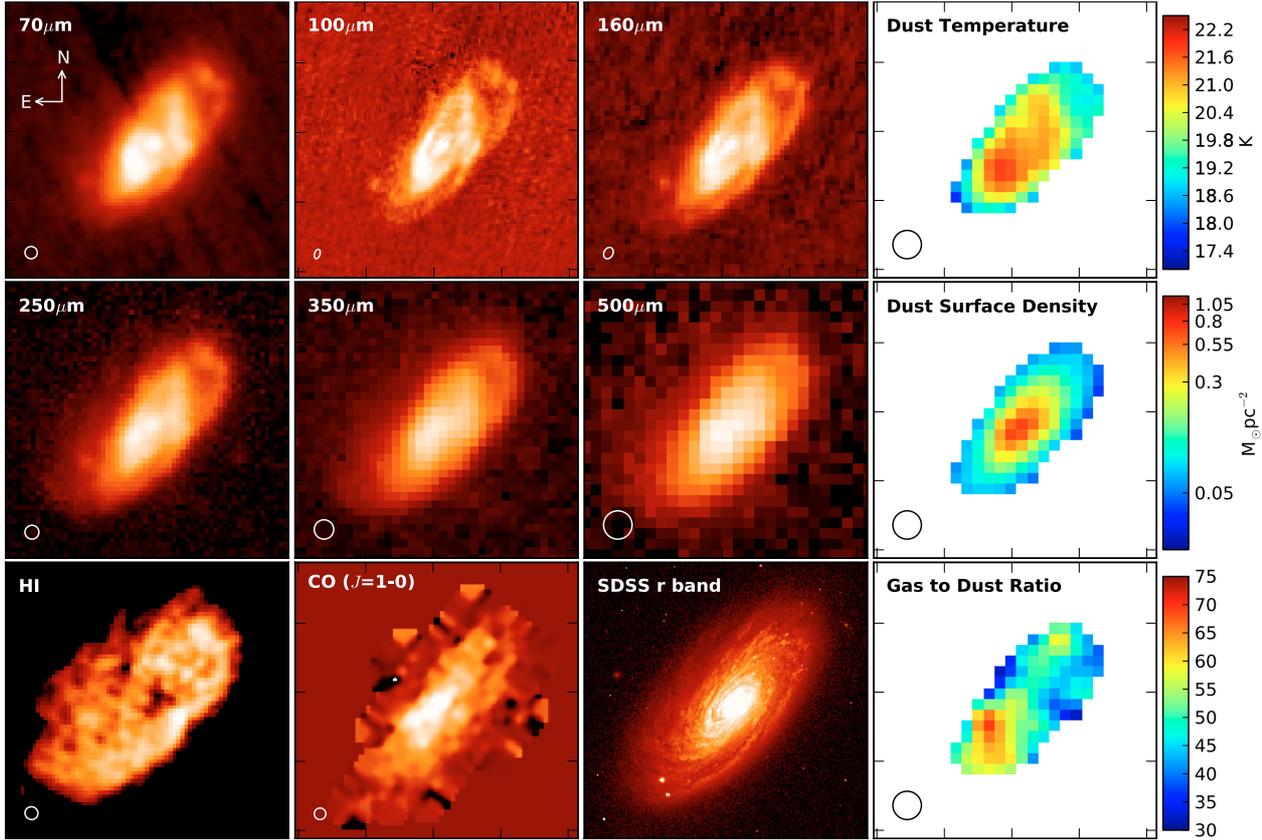
Fig. 2. Images of NGC 4501 in their native resolution and pixel size. The first three columns show the MIPS 70 μm PACS, SPIRE, and gas images on a log colour scale. The right-hand column shows maps of dust temperature, dust surface density (log scale), and gas-to-dust ratio. Beam sizes for the respective wavelengths are shown. The panels are 6′×6′ in size and centred on $12^h32^m00.0^s$, $+14^d25^m12.0^s$.

The uncertainties in the flux densities are calculated by adding in quadrature the calibration uncertainty, background subtraction uncertainty, and the uncertainty from the error map (created by the standard pipeline). For the pixels used in this analysis, the calibration uncertainty dominates for the PACS and SPIRE bands, except for the 500 μm band where the total uncertainty ranges from 15–23%. The average χ^2 value for all the fits is 2.5 with a standard deviation of 1.0, where the 90% confidence limit is 6.3 for 3 degrees of freedom. To obtain an estimate of the uncertainty in the fitted parameters, a bootstrap technique is used. This yields an average uncertainty in the pixel-by-pixel fitting of 1.0 K for temperature and 23% in the dust surface density.

4. Results

Maps of the cold dust temperature, dust-mass surface density, and gas-to-dust ratio are shown in Figs. 2 and 3, for NGC 4501 and NGC 4567/8, respectively. The extent of the maps corresponds to ∼65% of the optical radius. In each case, we find a centrally peaked, symmetrical distribution of dust mass in the galaxies. However, the dust temperature does not have the same symmetric distribution and varies across both galaxies, peaking at ∼22 K and decreasing to ∼19 K towards the outskirts of the galaxies. For NGC 4501, the peak of the dust temperature distribution corresponds to the bright spiral arm region seen to the southeast of the galaxy in the 70–160 μm images. For NGC 4567/8, the dust temperature distribution is also asymmetric, with higher temperatures in NGC 4568 that are coincident with peaks in the GALEX FUV. For both NGC 4501 and NGC 4567/8, the global temperature is 20 K (and also for NGC 4567 and NGC 4568, individually; we included an

additional uncertainty in the measurements to account for the overlap in emission from the two galaxies). In the regions that we analysed, we saw no evidence of any excess of flux at 500 μm that would imply an even colder dust component is present.

The dust-mass surface density distribution for both NGC 4501 and NGC 4568 has a smooth gradient, decreasing by a factor ∼4 from higher values at the centre to lower values in the outskirts. This is consistent with results found by Muñoz-Mateos et al. (2009), who find exponentially decreasing dust surface densities for the SINGS galaxy sample. For NGC 4501 and NGC 4567/8, we find global dust masses of $(1.2 \pm 0.3) \times 10^8$ $M_\odot$ and $(8.6 \pm 1.8) \times 10^7$ $M_\odot$, respectively ($(1.7 \pm 0.4) \times 10^7$ $M_\odot$ and $(6.6 \pm 1.5) \times 10^7$ $M_\odot$ for NGC 4567 and NGC 4568 individually, respectively).

For NGC 4501, the distribution of the gas-to-dust ratio is asymmetric, peaking in the southeast and varying by a factor ∼2 across the galaxy. The average gas-to-dust ratio for the pixel-by-pixel analysis is 52 ± 13 for NGC 4501, which is in good agreement with the global value of 51 ± 14. The variation in the gas-to-dust ratio within NGC 4501 is consistent with gas-to-dust profiles within our fitted radius for other Sb galaxies presented in Muñoz-Mateos et al. (2009). For NGC 4568, there is a large reduction in the HI-to-dust ratio in the central regions, which is probably due to higher molecular gas densities. The global (neutral) gas-to-dust ratios for NGC 4567 and NGC 4568 are 32 ± 12 and 39 ± 14, respectively. Though in all cases the global gas-to-dust ratios are low compared to the Galactic value, they are consistent with the lower end of the range of values in Draine et al. (2007) (correcting for the different X factor used). In Muñoz-Mateos et al. (2009), Sb and Sc galaxies have higher gas-to-dust ratios at larger radii than investigated
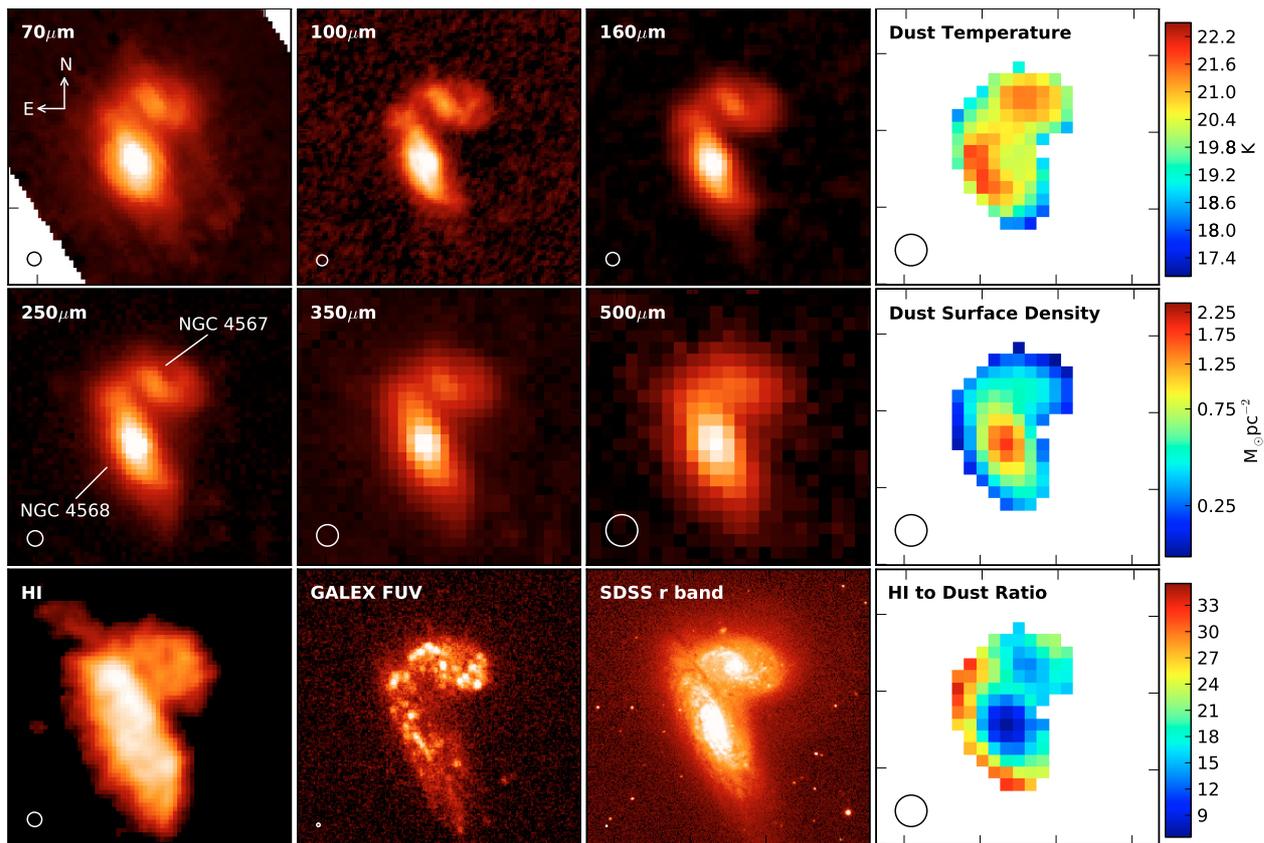
Fig. 3. Same as Fig. 2 but for NGC 4567/8. The GALEX FUV image has been smoothed slightly for display purposes. The panels are $5.4' \times 5.4'$ in size and centred on $12^h36^m33.6^s$, $+11^d15^m00.0^s$.

in the current work. For NGC 4501, the global value is in good agreement with the average pixel-by-pixel value, which suggests that a similar increase with radius may not be present for this galaxy. We note that since NGC 4501 and NGC 4568 are mildly HI deficient (0.4–0.6, Chung et al. 2009), low global gas-to-dust values of these Virgo galaxies could arise from the stripping of the outer gas and dust disk caused by environmental effects (Cortese et al. 2010). For the large sample of galaxies to be observed by HeViCS, we will be able investigate whether this is a general feature of the cluster environment.

5. Conclusions

We have fitted SEDs on a pixel-by-pixel basis to investigate the dust mass, temperature, and gas-to-dust ratios of NGC 4501 and NGC 4567/8. We have measured dust surface densities that peak at the centre of the galaxy and decrease towards the outer regions. In contrast, the temperature distribution is asymmetric, higher temperatures peaking at some distance away from the centre of the galaxy and then decreasing with increasing radius towards the outskirts. Once the full HeViCS observations are complete, we will be able to extend the analysis to larger radii and lower dust surface densities. For ~48 late-type galaxies with optical radii greater than 3′ to be observed with HeViCS, we will be able to begin to tackle questions about the dominant source of dust heating, how the dust interacts with the other phases of the ISM, and how morphology influences the dust distribution and temperature. By combining the results from HeViCS and the *Herschel* Reference Survey (Boselli et al. 2010), we will be able to study how environment affects the dust distribution and other properties of a galaxy.

References

Bendo, G. J., Wilson, C. D., Pohlen, M., et al. 2010a, A&A, 518, L65
Bendo, G. J., Wilson, C. D., Warren, B. E., et al. 2010b, MNRAS, 402, 1409
Boselli, A., Eales, S., Cortese, L., et al. 2010, PASP, 122, 261
Chung, A., van Gorkom, J. H., Kenney, J. D. P., Crowl, H., & Vollmer, B. 2009, AJ, 138, 1741
Cortese, L., et al. 2010, A&A, 518, L49
Davies, J. I., et al. 2010, A&A, 518, L48
Devereux, N. A., & Young, J. S. 1990, ApJ, 359, 42
Draine, B. T. 2003, ARA&A, 41, 241
Draine, B. T., Dale, D. A., Bendo, G., et al. 2007, ApJ, 663, 866
Gavazzi, G., Boselli, A., Donati, A., Franzetti, P., & Scodeggio, M. 2003, A&A, 400, 451
Gordon, K. D., Engelbracht, C. W., Fadda, D., et al. 2007, PASP, 119, 1019
Griffin, M. J., et al. 2010, A&A, 518, L3
Iono, D., Yun, M. S., & Ho, P. T. P. 2005, ApJS, 158, 1
Israel, F. 2000, in Molecular Hydrogen in Space, ed. F. Combes, & G. Pineau Des Forets, 293
Kenney, J., Beck, R., Helou, G., et al. 2006, in *Spitzer* Proposal ID #30945, 30945
Kennicutt, Jr., R. C., Armus, L., Bendo, G., et al. 2003, PASP, 115, 928
Kuno, N., Sato, N., Nakanishi, H., et al. 2007, PASJ, 59, 117
Mei, S., Blakeslee, J. P., Côté, P., et al. 2007, ApJ, 655, 144
Muñoz-Mateos, J. C., Gil de Paz, A., Boissier, S., et al. 2009, ApJ, 701, 1965
Pilbratt, G. L., et al. 2010, A&A, 518, L1
Poglitsch, A., et al. 2010, A&A, 518, L2
Roberts, M. S. 1962, AJ, 67, 437
Strong, A. W., & Mattox, J. R. 1996, A&A, 308, L21
Struck, C., Appleton, P., Charmandaris, V., Reach, W., & Smith, B. 2004, in *Spitzer* Proposal ID #3247, 3247
Whittet, D. C. B. 2003, Dust in the Galactic Environment, 2nd edn. (Bristol, United Kingdom: Institute of Physics Publishing)

Page 5 is available in the electronic edition of the journal at `http://www.aanda.org`

[1] School of Physics and Astronomy, Cardiff University, The Parade, Cardiff, CF24 3AA, UK
e-mail: Matthew.Smith@astro.cf.ac.uk

[2] Leiden Observatory, Leiden University, PO Box 9513, 2300 RA Leiden, The Netherlands

[3] Sterrenkundig Observatorium, Universiteit Gent, Krijgslaan 281 S9, 9000 Gent, Belgium

[4] Astrophysics Group, Imperial College London, Blackett Laboratory, Prince Consort Road, London SW7 2AZ, UK

[5] INAF - Osservatorio Astrofisico di Arcetri, Largo Enrico Fermi 5, 50125 Firenze, Italy

[6] Astronomical Institute, Ruhr-University Bochum, Universitäetsstr. 150, 44780 Bochum, Germany

[7] Laboratoire d'Astrophysique de Marseille, UMR 6110 CNRS, 38 rue F. Joliot-Curie, 13388 Marseille, France

[8] INAF - Osservatorio Astronomico di Padova, Vicolo dell'Osservatorio 5, 35122 Padova, Italy

[9] NASA *Herschel* Science Center, California Institute of Technology, MS 100-22, Pasadena, CA 91125, USA

[10] ESO, Alonso de Cordova 3107, Vitacura, Santiago, Chile

[11] Universita' di Milano-Bicocca, piazza della Scienza 3, 20100, Milano, Italy

[12] CAAUL, Observatório Astronómico de Lisboa, Universidade de Lisboa, Tapada da Ajuda, 1349-018, Lisboa, Portugal

[13] Institut d'Astrophysique Spatiale (IAS), Batiment 121, Universite Paris-Sud 11 and CNRS, 91405 Orsay, France

[14] Laboratoire AIM, CEA/DSM- CNRS – Université Paris Diderot, Irfu/Service d'Astrophysique, 91191 Gif-sur-Yvette, France

[15] Max-Planck-Institut fuer extraterrestrische Physik, Giessenbachstrasse, Postfach 1312, 85741, Garching, Germany

[16] INAF - Istituto di Astrofisica Spaziale e Fisica Cosmica, via Fosso del Cavaliere 100, 00133 Roma, Italy

[17] Institute of Astronomy and Astrophysics, National Observatory of Athens, I. Metaxa and Vas. Pavlou, P. Penteli, 15236 Athens, Greece

[18] Max-Planck-Institut für Astronomie, Köenigstuhl 17, 69117 Heidelberg, Germany